Title

Syk inhibition reprograms tumor-associated macrophages and overcomes gemcitabine-induced immunosuppression in pancreatic ductal adenocarcinoma

Journal

Cancer Research, 83(16)

ISSN

0008-5472

Authors

Rohila, Deepak

Park, In Hwan

Pham, Timothy V

et al.

Publication Date

2023-08-15

DOI

10.1158/0008-5472.can-22-3645

Syk inhibition reprograms tumor-associated macrophages and overcomes gemcitabine-induced immunosuppression in pancreatic ductal adenocarcinoma

Deepak Rohila[1], In Hwan Park[1], Timothy V. Pham[2], Jonathan Weitz[3], Tatiana Hurtado de Mendoza[3], Suresh Madheswaran[1], Mehreen Ishfaq[1], Cooper Beaman[1], Elisabette Tapia[1], Siming Sun[3], Jay Patel[3], Pablo Tamayo[2], Andrew M. Lowy[3], Shweta Joshi[1, *]

[1]Division of Pediatric Hematology-Oncology, Moores Cancer Center, University of California San Diego, CA, USA; [2]Office of Cancer Genomics, Moores Cancer Center, University of California, San Diego, CA, USA; University of California San Diego, CA, USA; [3]Department of Surgery, University of California, San Diego, CA 92093-0815, USA.

Correspondence to:

Shweta Joshi, Department of Pediatrics, Division of Pediatric Hematology-Oncology, Moores Cancer Center, University of California San Diego, La Jolla, CA 92093-0815, USA; shjoshi@health.ucsd.edu, Tel.: +1-858-822-7580

Running Title: Macrophage Syk drives PDAC progression.

Keywords: Macrophages, T cells, immune suppression, Syk, PDAC

Abbreviations: PDAC, pancreatic ductal adenocarcinoma; Syk, spleen tyrosine kinase; TME, tumor microenvironment; TAM, tumor-associated macrophage; TCM, tumor conditioned media; TGF beta, transforming growth factor; VEGF, vascular endothelial growth factor; BMDM, bone marrow-derived macrophages.

Disclosure of potential conflict of interest

No potential conflict of interest is disclosed by the authors.

Abstract

Pancreatic ductal adenocarcinoma (PDAC) is an insidious disease with a low five-year survival rate. PDAC is characterized by infiltration of abundant tumor-associated macrophages (TAMs) that promote immune tolerance and immunotherapeutic resistance. Here we report that macrophage spleen tyrosine kinase (Syk) promotes PDAC growth and metastasis. In orthotopic PDAC mouse models, genetic deletion of myeloid Syk reprogrammed macrophages into immunostimulatory phenotype, increased the infiltration, proliferation, and cytotoxicity of CD8+ T cells, and repressed PDAC growth and metastasis. Furthermore, gemcitabine (Gem) treatment induced an immunosuppressive microenvironment in PDAC by promoting pro-tumorigenic polarization of macrophages. In contrast, treatment with the FDA-approved Syk inhibitor R788 (fostamatinib) remodeled the tumor immune microenvironment, “re-educated” pro-tumorigenic macrophages towards an immunostimulatory phenotype and boosted CD8+ T cell responses in Gem-treated PDAC in orthotopic mouse models and an *ex vivo* human pancreatic slice culture model. These findings illustrate the potential of Syk inhibition for enhancing the anti-tumor immune responses in PDAC and support the clinical evaluation of R788 either alone or together with Gem as a potential treatment strategy for PDAC.

Significance: Syk blockade induces macrophage polarization to an immunostimulatory phenotype that enhances CD8+ T cell responses and improves gemcitabine efficacy in pancreatic ductal adenocarcinoma, a clinically challenging malignancy.

Introduction

Pancreatic ductal adenocarcinoma (PDAC) is an aggressive lethal malignancy with a mortality rate closely paralleling its incidence rates (1,2). With a five-year survival rate of 11%, PDAC represents the third leading cause of cancer-related deaths in the United States (3). Current standard therapies are not curative for advanced disease and minimally improve survival (4,5); hence novel therapies are urgently required to combat this devastating malignancy.

The characteristic features of PDAC are the presence of a highly desmoplastic stroma and extreme intra-tumoral heterogeneity, which drives immune and drug resistance in these tumors (6,7). Tumor-infiltrating immune cells of the myeloid lineage, including tumor-associated macrophages (TAMs), and myeloid-derived

suppressor cells (MDSCs), play crucial roles in generating an immunosuppressive microenvironment that diminishes effective anti-tumor immune responses in pancreatic cancer (8-11). Among these myeloid cells, $CD206^{+}MHCII^{-}$ TAMs are abundantly infiltrated in the PDAC tumors and promote PDAC growth (12). Emerging studies have shown that TAMs interact with the CD8+ T cells in the TME to reduce the mobility of T cells in the tumor stroma and limit their entry into the tumors (13). TAMs can also inhibit the function of CD8+T cells by secreting immunosuppressive cytokines like TGFβ (14) or limiting the metabolites required for T cell proliferation (L-arginine) by expressing arginase-1 enzyme (15). Recent studies have highlighted that gemcitabine (Gem) chemotherapy, the single most commonly used agent in PDAC, also promotes the polarization of macrophages to an immunosuppressive phenotype in the PDAC tumor microenvironment (TME), ultimately leading to Gem resistance (16,17). Consequently, approaches that modulate the pro-tumorigenic functions of TAMs have demonstrated that targeting these immune cells can unleash effector T cell responses and enhance responses to Gem treatment in PDAC (10,11,18,19).

We have recently shown that Syk signaling downstream of $\alpha_4\beta_1$ integrin promotes stabilization of hypoxia-inducible factor (HIF1α) to limit CD8+ T cell responses in lung adenocarcinoma (20,21). Moreover, using Syk inhibitor, R788 (fostamatinib), which is an FDA-approved drug for the treatment of patients with chronic immune thrombocytopenia (22), we have shown that Syk inhibition induces immunostimulatory transcriptional programming in macrophages to suppress tumor growth (20). The role of Syk in PDAC progression has not been previously explored in detail and one study reported that it acts as a tumor suppressor (23). For this reason, we sought to study the role of Syk in PDAC growth and metastasis.

Here we report that Syk is abundantly present in PDAC-associated macrophages and promotes polarization of macrophages into a pro-tumorigenic type, leading to immunosuppression, tumor growth, and metastasis in mouse models of PDAC. Using orthotopic mouse models and an organotypic PDAC slice culture model, we demonstrated that pharmacological inhibition of Syk using FDA-approved drug R788, reprogrammed TAMs towards immunostimulatory phenotype that promoted CD8+ T cell activation and improved responses to Gem. These results suggest the therapeutic potential of R788 alone or in combination with chemotherapy to augment anti-tumor immune responses in this cancer.

Materials and Methods

Human samples

Human tissues from deidentified patient samples were received from UC San Diego Moores Cancer Center Biorepository under IRB-approved protocol #181755.

Cell lines

The murine KPC1245 and KPC1242 pancreatic adenocarcinoma cell lines derived from $Kras^{G12D/+}$, $p53^{R172H/+}$, $Pdx1\text{-}Cre^{+}$ (KPC) mice (24) were a kind gift from Dr. David Tuveson (Cold Spring Harbor Laboratory, CSHL). The Panc02 cell line derived from C57BL/6 mice is described before (25). All cell lines were grown in Dulbecco's modified Eagle Medium (DMEM) media supplemented with 10% fetal bovine serum (FBS) and 1% penicillin and streptomycin (Panc02) or supplemented with sodium pyruvate, non-essential amino acids for KPC-derived cells. All cell lines were maintained at low passage numbers and were cultured at 37ºC and 5 % CO_2 in a humidified incubator. Cells were routinely tested for mycoplasma contamination and no cell manipulations were performed for this study.

Animals and *in vivo* experiments

All procedures involving animals were approved by the UCSD Animal Care Committee, which serves to ensure that all federal guidelines concerning animal experimentation are met. Floxed Syk mice, lysozyme M (LysM) Cre and CD19 cre recombinase transgenic mice were purchased from Jackson laboratories. $Syk^{fl/fl}$ mice were crossed with LysM cre or CD19 cre mouse models to specifically delete Syk from monocyte and macrophages ($Syk^{MC\text{-}KO}$ mice) (20) or from B cells ($Syk^{BC\text{-}KO}$mice) respectively. C57BL/6 mice used for drug treatment studies were obtained from Charles River Laboratories. Fifty thousand KPC1245 or KPC1242 cells and one million Panc02 cells were implanted orthotopically into the pancreata of 6-8 week old $Syk^{MC\text{-}WT}$ (aka $Syk^{BC\text{-}WT}$), $Syk^{BC\text{-}KO}$ and $Syk^{MC\text{-}KO}$ mice and C57BL/6 mice (25,26). The metastatic nodules on mesenteric lymph nodes and liver were counted under dissecting microscope. In some studies, C57BL/6 mice bearing PDAC tumors were treated with 50 mg/kg R788 (five times/ week) either alone or in combination with 15 mg/kg Gem (3 times/week) or in combination with 200µg anti PDL1 mAb (clone 10F.9G2, BioXCell), or isotype control LTF2

(BioXcell). R788 was obtained from Selleck Chemicals (Houston, TX) and Gemcitabine-HCL was purchased from Biotang (Waltham, MA, USA). CD11b+F4/80+ macrophages were isolated using CD11b and F4/80 magnetic beads (Miltenyi Biotec, San Diego) according to manufacturer's instructions.

Macrophage-depletion and CD8+ T cell depletion experiments

For macrophage depletion experiments, mice bearing KPC1245 tumors were treated with 50 mg/kg of anti-CSF1R antibody (clone AFS 98, BioXcell, administered intraperitoneally, every alternate day, until tumors were harvested on day 15. For CD8 depletion experiments, mice with KPC1245 tumors were treated with 200µg of anti-CD8 (clone YTS169.4) or an isotype rat IgG2b control (LTF-2) from Bio-X-Cell administered ip on day -3, 0, 3, 6 and 10 of tumor inoculation as described before (20).

Cell Proliferation Assay

KPC1245 cells were plated at 4 x 10^4 cells/well in 96-well plates in media containing DMEM+10% FBS. Cells were incubated overnight and treated with DMSO or R788 for 48 hr. Cell viability assay was performed using AlamarBlue® (Roche) according to the manufacturer's protocol.

Single-cell preparation for flow cytometry

Single cell suspensions from tumors were prepared as described before (20). Briefly, tumors were isolated, minced, and incubated for 30-45 min at 37°C in a dissociation solution containing Hanks Balanced Salt Solution supplemented with 0.5 mg/ml collagenase IV (Sigma), 0.1 mg/ml hyaluronidase V (Sigma), and 0.005 MU/ml DNAse I (Sigma). The undigested tissues were removed by passing through 70 µm nylon mesh and centrifuged at 1500 rpm for 5 min. The red blood cells were lysed using RBC lysis buffer (Pharm Lyse, BD Biosciences, San Jose, CA, USA) and cells were prepared for flow cytometry.

Flow cytometry

For flow cytometry staining, dissociated cells were incubated with a fixable viability stain 510 (BD, Biosciences) followed by staining with primary antibodies directed against CD45 (30-F11), CD11b (M1/70), Gr1 (RB6-8C5), F4/80 (BM8), CD206 (C068C2), MHCII (AF6-120.1), CD44 (IM7), PDL1 (MIH5), TIGIT (1G9), CD69 (H1.2F3) obtained from BD Biosciences; CD3 (145-2C11), CD4 (GK1.5), CD8 (53-6.7), $pSyk^{Y348}$ (moch1ct) from eBioscience, PD1 (29F.1A12), and CD62L (MEL-14) from Biolegend. Samples were acquired on BD

Fortessa or LSRII and data were analyzed using FlowJo software version 10 (Treestar, Ashland, OR, USA).

Immunohistochemistry and Immunofluorescence

Formalin fixed paraffin embedded (FFPE) tissue sections (4μm) of human PDAC were obtained from UC San Diego Moores Cancer Center Biorepository. Formalin-fixed paraffin-embedded (FFPE) tissue sections (4μm) of human PDAC or mouse tumors were used for immunohistochemistry (IHC) or immunofluorescence (IF) studies. Slides were baked overnight and then either stained for H and E staining or Trichome staining or processed for IHC and IF staining. For IHC studies, human samples were stained with the following antibodies: anti-CD20 (ab64088, 1:100, Abcam), anti-CD68 (MA5-12407, 1:50, Invitrogen), anti-CD206 (ab64693, 1:100, Abcam), anti-CD3 (ab16669, 1:500, Abcam), anti-CD4 (ab288724, 1:1000, Abcam), anti-CD8 (70306S, 1:50, Cell Signaling). Mouse tumors were stained with the following antibodies: anti-SMA (ab5694, 1:1000, Abcam), anti-CD3 (ab16669, 1:500, Abcam) anti-CD8 (14-0195-82, 1:50, Invitrogen), anti-B220 (553086, 1:200, BD Pharmingen), and anti-CD68 (ab125212, 1:50, Abcam). Antigen retrieval was carried out in citrate buffer (pH 6.0, Vector Laboratories) at 95°C for 30 min. After antigen retrieval, tissue sections were incubated with BLOXALL (Vector Laboratories) for 10 min followed by blocking Blotto (Thermo) for 10 min. Sections were stained with primary antibodies at recommended dilutions in Blotto for 1 hr at room temperature. After washing primary antibodies, the samples were stained with anti-mouse or anti-rabbit secondary antibodies HRP Polymer (Cell IDX for 30 min at RT followed by DAB staining using DAB chromogen (VWR, 95041-478) for 5 min. The images with positive staining were captured using Olympus inverted microscope. The whole area of the tumor was selected as a field of interest, and the area with immunohistochemically positive staining within the field of interest was calculated by the Image J software after setting the thresholds. The results are expressed as the percentage of the positively immunolabelled area within the total area of the tumor. For immunofluorescence staining, antigen retrieval was carried out as described above followed by blocking with Blotto for 10 min. The tissues were then incubated with Syk (clone EP573Y, ab40781, 1:1000, Abcam) and CD68 (MA5-12407, 1:50, Invitrogen) antibodies in Blotto for 1 hr at room temperature. After two washings with 1X TBST buffer, samples were stained with anti-mouse or anti-rabbit HRP polymer-conjugated secondary antibodies (Cell IDX) for 30 min at RT. Tissues were then incubated with Alexa Fluor 488 and Alexa Fluor 594 Tyramide reagents (Thermo) for 10 min. DAPI was used to counterstain the nuclei. For some

studies, the slides were deparaffinized, and rehydrated, followed by antigen retrieval in citrate buffer. The slides were bleached with 4.5% H_2O_2 and 24 mM NaOH in PBS with exposure to light. After 45 minutes the bleaching solution was refreshed, and bleaching was continued for 45 more minutes. The slides were then blocked followed by incubation with the following antibodies; anti-CD8a (14-0808-82, 1:400, Invitrogen) and anti-Ki67 (ab16667, 1:200, Abcam) detected with donkey anti-rat AF647 (A48272, 1:500, Invitrogen) and donkey anti-rabbit (A10042, 1:500, Invitrogen, anti-CD31 (DIA-310, 1:200, Dianova) detected with donkey anti-rat AF647 (A48272, 1:500, Invitrogen), anti-F4/80 (70076S, 1:200, Cell Signaling) detected with goat anti-rabbit AF647 (A32733, 1:500, Invitrogen).The images of fluorescent staining were captured using Keyence BZX-700 fluorescent microscope.

Macrophage polarization studies

Bone marrow derived macrophages (BMDMs) were generated from C57BL/6 mice as described before (21). Tumor conditioned media (TCM) was prepared from confluent KPC1245 cells. For this, cells were grown to 80% confluence, washed with PBS and media changed to DMEM without FBS for another 48 hrs. TCM was collected after 48 hrs. and used for co-culture experiments. For inhibitor studies, BMDMs stimulated with 20ng/ml IL4, or WT BMDMs incubated with TCM from KPC1245 cells were treated with 500nM R788 for 24 hrs followed by RNA isolation.

Syk activation studies

TAMs were isolated from Panc02 PDAC tumors based on FACS sorting of cells stained with CD11b and F4/80. TAMs were stimulated for Fc gamma ligation or LPS or $\alpha_4\beta_1$ integrin stimulation. For Fc gamma ligation, cells were incubated with purified rat anti-mouse CD16/CD32 (BD Pharmingen) at 1.0 µg/10^6 cells for 10 min 4°C and then incubated with goat anti-rat F(ab')2 (25 µg/ml, Jackson ImmunoResearch) for 10 min followed by lysate preparation. For TLR4 signaling, TAMs were stimulated with 1µg/ml of LPS for 10 min, followed by lysate preparation. For $\alpha_4\beta_1$ integrin studies, non-tissue culture petri dishes were coated with 10 ug/ml of H296 (ligand for $\alpha_4\beta_1$ integrin) in PBS for 1 hr, followed by washing with PBS and plating of cells for 10 min and lysate preparation.

Western blot analysis

BMDMs, CD90.2 + T cells, CD19+ B cells isolated from splenocytes of PDAC-bearing mice, *in vitro* cultured Panc02, KPC1245 cells and CD11b+F4/80+ TAMs stimulated with LPS or by Fc gamma ligation or $\alpha_4\beta_1$ integrin ligation were solubilized in RIPA buffer containing protease and phosphatase inhibitors. Proteins were run on SDS-PAGE gels, electro transferred to nitrocellulose membranes and were immunoblotted with antibodies from $pSyk^{Y348}$ (Abcam), Syk (Santa Cruz), β-actin (Santa Cruz) as described before (21).

Real Time PCR

Total RNA was isolated from BMDMs or murine or human PDAC slices using the Qiagen RNAeasy kit (Qiagen, Hilden, Germany) and cDNA was prepared using iscript cDNA synthesis kit (Bio-Rad, Hercules, CA). cDNA was amplified by RT-PCR reactions with 1× SYBR green supermix (Bio-Rad, Hercules, CA) in 96-well plates on an CFX96 Real time system (Bio-Rad, Hercules, CA), using the program and the custom designed primers obtained from Integrated DNA Technologies. Relative expression levels were normalized to Gapdh expression as previously described (20).

Organotypic slice culture

Human PDAC slices and slices derived from eight-nine week old KPC mice-a genetically engineered mouse model (GEMM) were cultured as described previously (27,28). The tissues were first sectioned into fragments (approximately 5-10 ml cubed) and imbibed in low melting agarose followed by cutting 200μm sections using a vibroslicer (VT1000P; Leica Biosystems). The slices were transferred into 0.4μm trans well cell culture inserts (Cat# CLS3450-24EA) containing RPMI media and incubated with either 250 nM Gem or 2.5 μM R788 or combination of Gem and R788. The media was changed the next day and after three days of culture, supernatants were used for cytokine ELISA and slices were used for RNA isolation or immunohistochemistry.

ELISA assays

Tissue culture supernatants from PDAC slices were assayed for total TGF-β1 or MCP1 (CCL2) by using commercially available Legend Max ELISA kits from BioLegend (San Diego, CA) according to manufacturer's instructions.

Gene expression analysis

Gene expression microarray data and sample information of matched tumor and normal samples from 36 Pancreatic Adenocarcinoma patients were downloaded from Gene Expression Omnibus (GEO) accession GSE15471 (29). Sequence analysis on IL-4 polarized BMDMs from $Syk^{MC\text{-}WT}$ and $Syk^{MC\text{-}KO}$ mice was performed as described previously (20). Briefly, RNAseq expression data of IL-4 polarized BMDMs from $Syk^{MC\text{-}WT}$ and $Syk^{MC\text{-}KO}$ were downloaded from GEO accession GSE115109 (20) and aligned using a STAR (30) to the mm10 mouse reference genome with reads quantified by Salmon (31) in a standard RNAseq BCBio pipeline workflow. Differential gene expression in the IL4-exposed $Syk^{MC\text{-}WT}$ and $Syk^{MC\text{-}KO}$ BMDMs were compared using DESeq2 (32) with apeglm being used for empirical shrinkage effect size estimation (33). P-values were multiple hypotheses corrected using the Benjamini-Hochberg method in the python stats models package. The heatmap of relevant differentially expressed genes was made using the Python seaborn package. The results are available at GSE115109.

Sc-RNA-Seq data acquisition, integration, and analyses

Single-cell RNA-seq data from 24 human PDAC tumor samples and 11 normal pancreases were downloaded from GSA accession CRA001160 along with sample information and cell identity metadata, available at https://ngdc.cncb.ac.cn/gsa/browse/CRA001160. The cells for each sample were separated, and counts of each gene from cells of the same type were averaged (sum of gene counts/number of cells of type in sample); non-immune cells were grouped together in the non-immune category for clarity. Finally, a box plot of SYK expression across the different cell types was generated and p-values between each cell type were computed using the Kruskal-Wallace paired sample test due to the paired nature of the data.

Statistical analysis

For all *in vitro* studies, experiments were performed three or more times with three or more biological replicates per group. All *in vivo* experiments were performed at least twice with 8-10 animals assigned/group. Data were normalized to standard where applicable. Significance testing was performed by one-way ANOVA with Tukey's post-hoc testing for multiple pair-wise testing with more than two groups and by student's t-test when only two groups were compared. Statistical analysis was performed using GraphPad Prism V.9 software. Unless otherwise stated, data are shown as mean ± SEM. In all cases, * $p < 0.05$, ** $p < 0.01$ *** $p < 0.001$, **** $p < 0.0001$, ns = not significant.

Data availability statement

Gene expression microarray data of matched tumor and normal samples from Pancreatic Adenocarcinoma patients were downloaded from Gene Expression Omnibus (GEO) accession GSE15471. RNAseq expression data of IL-4 polarized BMDMs from $Syk^{MC\text{-}WT}$ and $Syk^{MC\text{-}KO}$ were downloaded from GEO accession GSE115109. Single-cell RNA-seq data from human PDAC tumor samples and normal pancreases were downloaded from accession CRA001160 available at https://ngdc.cncb.ac.cn/gsa/browse/CRA001160. All other raw data are available upon request from the corresponding author.

Results:

Syk positive macrophages accumulate in murine and human PDAC

Tumor associated macrophages are principal regulators of tumor progression and chemo- and immunotherapeutic resistance in PDAC (8-10,34). Similar to previous reports (11,35) demonstrating the increased infiltration of TAMs into pancreatic tumors, we also observed an increase in the presence of CD68+ macrophages in human PDAC compared with healthy pancreatic tissue (Fig. 1A). To examine the accumulation of macrophages in murine PDAC, we orthotopically implanted KPC1245 and KPC1242 cells in C57BL/6 mice. Immunostaining of pancreata from normal and tumor-bearing mice revealed that F4/80+ macrophages are abundantly infiltrated in KPC1245 and KPC1242 tumors (Supplementary Figs. S1A-B). In addition, we found that macrophages are crucial regulators of PDAC growth as administration of anti-mouse anti-CSF1R suppressed tumor growth in mice bearing KPC1245 tumors (Supplementary Figs. S2A-C).

Based on the abundance of macrophages in PDAC, we sought to test if Syk, is expressed in PDAC and if therapeutic targeting of this kinase is efficacious in treating this recalcitrant neoplasm. We found an abundant increase in SYK+ cells in the tissue sections of invasive human PDAC as compared to normal tissue using immunofluorescence microscopy (Fig. 1B). Correspondingly, analysis of the publicly available dataset, GSE15471, and single cell RNAseq data set (accession number: CRA001160) revealed high expression of SYK in human PDAC as compared to normal pancreas (Figs. 1C and D).

Like human PDAC, *Syk* levels were high in murine PDAC tumors compared to normal pancreatic tissue (Supplementary Fig. S3A). *Syk* was expressed specifically in CD45+ immune cells isolated from orthotopically implanted KPC1245 tumors and minimally in CD45- tumor cells as revealed by RTPCR (Supplementary Fig.

S3B). Most notably, we observed the presence of Syk in CD11b+F4/80+ TAMs isolated from murine PDAC tumors (Fig. 1E). Syk is also expressed in CD19+ B cells isolated from spleens of mice bearing PDAC tumors and to a lower extent in BMDMs. However, Syk is not expressed in murine PDAC cell lines, Panc02 and KPC1245 and CD90.2+ T cells from spleens of mice bearing PDAC tumors (Fig. 1E). Likewise, the analysis of sc-RNA-seq data (CRA001160), revealed that Syk is maximally expressed in macrophages, followed by B cells and non-immune cells while not in T cells from human PDAC (Fig. 1F). Immunofluorescence microscopy also confirmed immunoreactivity of Syk in CD68+ TAMs in the tissue sections of human PDAC specimens (Fig. 1G).

In macrophages, Syk is known to be activated upon binding to phosphorylated ITAMs of Fc gamma receptor, or by binding to the cytoplasmic domains of integrin adhesion receptors, most notably β_1 and β_3 integrin or by TLR4 (36,37). We have previously shown that $\alpha_4\beta_1$ integrin can maximally activate Syk at Y348 site in TAMs isolated from the lung adenocarcinoma tumors (20). Here, we found that macrophages in PDAC tumors showed higher expression of $pSYK^{348}$ as compared to macrophages from normal pancreas (Fig. 1H). In addition, TAMs are activated downstream of $\alpha_4\beta_1$ integrin and Fc gamma receptors in the PDAC TME, with no activation by TLR4-mediated signaling (Fig. 1I). Taken together, these results clearly indicate that Syk is abundantly present in PDAC-associated-macrophages and is activated downstream of $\alpha_4\beta_1$ integrin or/and Fc gamma receptors in the PDAC TME and may function to modulate PDAC growth and metastasis.

Macrophage Syk promotes PDAC growth and metastasis and limits infiltration, proliferation, and activation of CD8+ T cells in the PDAC TME

As Syk is abundantly present in macrophages and to some extent in B cells (Fig.1E and F), we next investigated if deletion of Syk in macrophages or B cells can impede PDAC growth. For this study, we used our previously established conditional myeloid Syk KO mice ($Syk^{MC\text{-}KO}$) (20) and recently generated B cell Syk KO ($Syk^{BC\text{-}KO}$) mice and examined tumor growth of two syngeneic murine PDAC cell lines: KPC1245 and Panc02 according to the depicted schema (Fig. 2A). We found that CD19+ B cells were significantly reduced in $Syk^{BC\text{-}KO}$ mice, but tumor growth is similar in $Syk^{BC\text{-}WT}$ and $Syk^{BC\text{-}KO}$ mice implanted with orthotopic KPC1245 tumors (Supplementary Figs. S4A-C), suggesting that Syk deletion in B cells is not responsible for PDAC growth. However, we found that both orthotopic Panc02 and KPC1245 pancreatic tumors from $Syk^{MC\text{-}KO}$ mice

were significantly smaller than pancreatic tumors from $Syk^{MC\text{-}WT}$ mice (Fig. 2B and C). Remarkably, the prevalence of metastases in colonic lymph nodes and liver was also substantially reduced in pancreatic tumors from $Syk^{MC\text{-}KO}$ mice, indicating that myeloid Syk promotes PDAC growth and metastatic progression (Fig. 2B and C). Analysis of pancreata from KPC1245-bearing mice by immunofluorescence or immunohistochemistry reveals that $Syk^{MC\text{-}WT}$ animals exhibited abundant expression of smooth muscle actin (SMA) and Trichrome, as well as increased CD31 staining (Fig. 2D), suggesting a role for myeloid Syk in promoting desmoplasia.

As myeloid Syk deletion has significant impact on PDAC growth (Figs. 2B & C), we analyzed alterations in immune cells in tissues from PDAC-bearing $Syk^{MC\text{-}WT}$ and $Syk^{MC\text{-}KO}$ mice by flow cytometry. We found that Syk deletion has no significant impact on the recruitment of CD19+ B cells, CD11b+Gr1- monocytes, CD11b+Gr1+ granulocytes and $CD11b^{+}Gr1^{-}F4/80^{+}$ TAMs into PDAC tumors (Supplementary Figs. S5A-D). Importantly both Panc02 and KPC1245 PDACs from $Syk^{MC\text{-}KO}$ mice exhibited significantly more CD3+ and CD8+ T cells than PDACs from $Syk^{MC\text{-}WT}$ mice (Figs. 2E-F), with no significant impact on the systemic infiltration of T cells in the spleens of tumor bearing $Syk^{MC\text{-}WT}$ and $Syk^{MC\text{-}KO}$ mice (Supplementary Figs. S6A-D). We found a significant increase in the T cell chemo attractants CXCL5, CXCL9 and CXCL10 in the $Syk^{MC\text{-}KO}$ treated tumors (Supplementary Fig. S6E). In addition to increased infiltration, CD8+T cells proliferate in the $Syk^{MC\text{-}KO}$ treated tumors (Fig. 2G). Accordingly, T cells isolated from the PDAC-bearing $Syk^{MC\text{-}KO}$ mice showed higher expression of *Ifng*, *Gzmb* and *Prf* (Fig. 2H). These results clearly suggest that myeloid Syk promotes immunosuppression, PDAC growth, and metastasis.

Syk enhances an immunosuppressive phenotype of macrophages *in vitro and in vivo*

Since we observed that Syk deletion promotes recruitment and activation of T cells in PDAC, we postulated that Syk promotes immunosuppressive programming of macrophages to impede CD8+ T cell responses in PDAC. We found that Syk deletion reprogramed TAMs towards immunostimulatory phenotype as we observed an increase in the frequency of $MHCII^{+}$ TAMs with a concomitant reduction in $CD206^{+}$ immunosuppressive TAMs in PDAC tumors from $Syk^{MC\text{-}KO}$ mice (Figs. 3A and B). Similarly, we found higher expression of immunosuppressive genes in TAMs isolated from KPC1245 tumors implanted in $Syk^{MC\text{-}WT}$ mice while TAMs sorted from $Syk^{MC\text{-}KO}$ mice showed higher expression of proinflammatory genes like *Il12*, *Ifng*, *Nos2*, as shown by RTPCR (Fig. 3C). We next determined if Syk can regulate the transcriptional programming

in macrophages *in vitro*. It is well-documented that incubation with IL4 or TCM promotes immune suppressive polarization of macrophages *in vitro* (38). RNA-seq data revealed that IL4 stimulated $Syk^{MC\text{-}WT}$ BMDMs exhibited higher expression of genes related to immune suppression such as *Ido1*, *Vegfd*, *Arg1*, and *Ccl2* as compared to IL4 stimulated $Syk^{MC\text{-}KO}$ BMDMs (Fig. 3D). Interestingly, we also found higher expression of genes related to metastasis, such as *Pdgfa, Pdgfb* (39), in IL4 stimulated $Syk^{MC\text{-}WT}$ BMDMs, which may help explain the increased metastasis observed in $SYK^{MC\text{-}WT}$ mice (Figs. 2 B and C). We next asked if pharmacological inhibition of Syk can reduce pro-tumorigenic polarization of macrophages *in vitro*. For this, we used a commercially available Syk inhibitor, R788 has an IC50 of 41 nM for Syk with no inhibition of ZAP-70 and Lyn kinases (22). We observed that R788 prevented IL4-induced expression of immunosuppressive genes (Fig. 3E). While co-culture of BMDMs with TCM from KPC-1245 tumor cells increased the gene expression of *Il6, Il10, Ccl2, Arg, Tgfb, Mmp9, and Vegf*, R788 downregulated the expression of these genes (Fig. 3F). Taken together, these results indicate that Syk inhibition reduces expression of immune suppressive genes and stimulates expression of proinflammatory genes in macrophages, which likely contribute to enhanced CD8+T cell recruitment, proliferation, and activation in PDAC tumors.

To investigate if deletion of Syk specifically in macrophages is sufficient to block PDAC growth, we treated $Syk^{MC\text{-}WT}$ and $Syk^{MC\text{-}KO}$ mice bearing KPC1245 tumors with R788. We found that administration of R788 significantly reduced tumor growth in $Syk^{MC\text{-}WT}$ mice (Figs. 3G). However, R788 further did not significantly reduce tumor growth in $Syk^{MC\text{-}KO}$ mice (Fig. 3G). As Syk is predominantly expressed in CD45+ immune cells in PDAC tumors (Fig. S2B) with no contribution of B-cell Syk in PDAC growth (Fig. S4C) and minimal effect of Syk inhibitors on PDAC cells *in vitro* (Supplementary Fig. S7), we conclude that macrophage Syk promotes immunosuppression and PDAC growth.

Syk inhibition with FDA-approved drug R788 synergizes with Gem to suppress PDAC growth and metastasis

As Syk controls immunosuppressive programming of macrophages, we speculated that Syk inhibitors either alone or together with immunotherapy or chemotherapy will improve the outcomes of pancreas cancer. To test this hypothesis, Panc02, and KPC1245 cells were orthotopically injected into the pancreata of WT mice, and mice were then treated with R788 either alone or in combination with anti-PDL1 mAb or Gem,

according to the schema as depicted in Fig. 4A. We observed that vehicle mice developed large pancreatic tumors with numerous metastatic nodules in liver and colon, whereas R788 treated tumors were significantly smaller with rare metastatic nodules (Figs. 4B-D). We found that antibodies targeted against programmed death ligand 1 (anti-PDL1 mAb) either alone or in combination with R788 significantly reduced tumor growth in the Panc02 PDAC (Fig. 4B). However, no significant synergy was observed between anti-PDL1 mAb and R788 in the KPC1245 PDAC (Fig. 4C-D). We found that PDL1 is expressed both on CD45- tumor cells and CD45+ TAMs, and R788 didn't impact the expression of PDL1 either on macrophages or on TAMs (Supplementary Fig. S8) which explains the lack of synergy between R788 and anti-PDL1 mAb in KPC1245-treated tumors. However, we found that R788 synergizes with Gem to reduce tumor growth, and metastasis in Panc02, KPC1245, and in another KPC-derived cell line, KPC1242 (Figs. 4B-E). In addition, histological evaluation of KPC-1245 tumors from Gem and R788 treated mice showed reduced desmoplasia as revealed by Trichome staining (Fig. 4F).

Gem endows TAMs with pro-tumorigenic properties but R788 reprograms TAMs to overcome Gem-induced immunosuppression in PDAC in a CD8+T cell dependent manner

Several studies have shown that macrophage infiltration and macrophage-induced immunosuppression both contribute to Gem resistance in PDAC (16,17). As Syk inhibition reduced immune suppressive polarization of macrophages *in vitro* and *in vivo* (Fig. 3), we investigated if R788 can overcome Gem-induced immunosuppression and can boost CD8+ T cells responses in these tumors. We found that treatment of KPC1245 tumors with R788 or Gem did not significantly reduce infiltration of total CD45+ cells, while there is significant decrease in CD11b+ cells on R788 treatment (Figs. 5A-B). Most notably, Gem treatment reduced infiltration of TAMs but has no impact on the infiltration of $CD206^{+}$ immunosuppressive TAMs in the PDAC tumors while R788 alone or together with Gem significantly reduced the infiltration of CD206+ TAMs in the tumor bed (Figs. 5C-D). In addition, Gem-treated tumors show increased gene expression of *Arg*, *Il10*, *Tgfb* and *Ccl2* as compared to vehicle tumors and R788 reduced Gem-induced immunosuppressive transcription in these tumors (Fig. 5E).

Remarkably, we observed that R788 treatment increased infiltration of CD8+ T cells as compared to vehicle tumors (Figs. 5F-H). Furthermore, these CD8+ T cells are more proliferative in the R788 treated group

or Gem + R788-treated group as compared to vehicle or Gem (Fig. 5G). In addition, PDAC infiltrating CD8+ T cells were highly activated in R788 and Gem + R788 treated group as they exhibit increased infiltration of CD44+CD62L- effector T cells and CD69+ T cells as well as enhanced gene expression of *Ifnγ* and *Gzm* in treated tumors (Fig. 5H-I). Similarly, we found higher infiltration of CD69+ CD8+ T cells in the R788-treated KPC1242 tumors (Supplementary Fig. S9A-B). Most notably, we didn't observe any significant changes in the expression of exhaustion markers PD1 and TIGIT on tumor infiltrating CD8+ T cells in the R788-treated tumors (Supplementary Fig. S9C-D). We found that depletion of CD8+ T cells in R788-treated tumors or Gem + R788 treated tumors restored the tumor growth in both groups, with no changes in tumor growth in the Gem-treated group (Fig. 5 J), elucidating that synergy between Gem and R788 treatment is CD8+T cell dependent. Altogether these results indicate that Gem treatment promotes immune suppressive polarization of macrophages (this is actually a wound-healing response), but when combined with Syk inhibitors it remodels the TME towards immune stimulation, boosted T cell proliferation and activation to improve anti-tumor immune responses in PDAC.

R788 remodels the immune microenvironment in ex-vivo murine and human PDAC slice cultures

To determine whether R788 together with Gem can improve anti-tumor immune responses in spontaneous murine models and human PDAC, we employed a tumor slice culture model as shown in Fig. 6A. Similar to the results observed in mouse orthotopic tumor models, we found that slices derived from KPC GEMM mouse tumors and treated with Gem showed increased expression of *Arg*, *Vegf*, *Tgfβ*, *Ccl2,* and *Il10* as compared to vehicle slices, showing immunosuppressive TME in Gem-treated tumor slices (Figs. 6B-F). However, the treatment of these slices with R788 downregulated the expression of these immunosuppressive genes (Figs. 6B-F) and upregulated the expression of *Ifng*, and *Gzmb* (Fig. 6G-H). R788 and Gem treatment also reduced the protein expression of MCP1 (CCL2) (Fig. 6I).

Similarly, treatment of human PDAC slices with Gem and R788 led to the reduction in the mRNA expression of *ARG1*, *VEGF*, *IL10*, and *TGFB* in three different patient PDAC samples (Fig. 7A-C, Table S1) and decreased the secretion of TGFβ (Supplementary Fig. S10). We also found that R788 treatment alone was able to reduce the CD206+ TAMs without any significant changes in the number of CD68+ macrophages as shown by immunohistochemistry (Figs. 7D-E). Most notably, we also observed an increase in the number of

CD8+ T cells in R788-treated slices as well as Gem + R788- treated slices suggesting an effect on T cell proliferation (Figs. 7D-F).

Discussion

PDAC tumors exhibit profound infiltration of macrophages, which promote immunosuppression, and relapse from therapy (12,18). It is now well accepted that relieving the immunosuppressive activities of these cells to enhance cytotoxic T cell activity and to mobilize CD8+T cells in the tumor stroma, can prove useful for mounting durable anti-tumor immune responses (10,11). Here, we have identified Syk as a potential regulator of immunosuppression and metastasis in pancreatic cancer. Contrary to a previous study by Layton et al (23), we found higher expression and activation of Syk in CD68+ TAMs infiltrating in mouse and human PDAC, with no expression of Syk in pancreatic cell lines. We found that macrophage Syk plays a critical role in regulating PDAC growth and metastasis. Our studies reveal that Syk promotes immunosuppressive transcriptional programming of macrophages by stimulating the expression of *Arg*, *Ccl2*, *Il10, Mmp9,* and *Tgfβ.* In contrast, inhibition of this kinase increased the expression of *Il12*, *Ifng*, and *Nos2* and skewed the macrophages toward an immunostimulatory phenotype *in vitro* and *in vivo*. This reprogramming of macrophages towards an immunostimulatory phenotype in Syk-inhibitor treated tumors was accompanied by increased CD8+ T cell recruitment to PDAC tumors, enhanced CD8+ T cell proliferation, increased T cell expression of *Ifng*, *Gzm,* and *Prf* and bolstered CD8+ T cell responses in the PDAC tumors. We found that Syk inhibitors synergize with Gem to slow PDAC growth in a T-cell dependent manner. Finally, using slice cultures established from resected human PDAC tumor specimens, we show that Syk inhibitors, either alone or in combination with Gem, decrease the expression of markers associated with an immunosuppressive phenotype.

Syk can be activated downstream of various receptors and play diverse biological functions (36). Similar to our observation in lung adenocarcinoma tumors (20), macrophage Syk is activated downstream of $\alpha_4\beta_1$ integrin in the PDAC tumors. In contrast to lung tumors, Syk is also activated downstream of Fc gamma receptors in the PDAC TME. In a related study, BTK-mediated signaling in B cells and FcRγ positive macrophages promotes PDAC growth (10). While, we have not evaluated the Syk-mediated crosstalk between B cells and FcRγ-positive macrophages in PDAC, we observed that Syk signaling in B cells have no role in PDAC growth. Though B cells, are reported to play a protumorigenic role in PDAC progression (10,40), there

are discrepancies in the literature regarding their role, and a recent study has shown that B cells do not favor PDAC progression (41). However, the role of regulatory B cells (Breg) in promoting PDAC progression and immunosuppression has recently been reported by several groups (40,42). It might be feasible that similar to BTK, Syk has a role in regulating Breg-mediated immunosuppression in PDAC. In our studies, we used CD19 cre mice that depletes all mature and immature B cells and not specifically the Breg population. Hence, future studies will be focused on using specific strategies to deplete Bregs to study the role of Syk in Breg differentiation and Breg-mediated immunosuppression in PDAC.

We demonstrated that administration of anti-PDL1 mAb alone reduced tumor growth in orthotopic mouse models as reported before (43-45). However, we didn't observe additive effects of targeting Syk and PDL1 together in PDAC. These findings are similar to our studies in the B16 melanoma model, where we demonstrated that Syk inhibitors and anti-PDL1 mAb alone reduced tumor growth but combination of R788 and anti-PDL1 showed no significant additive effect (20). Interestingly, in related studies, PI3K gamma inhibitors or BTK inhibitor ibrutinib reprogrammed the macrophages and slowed PDAC growth but showed no additive effects in combination with immunotherapies (10,11).

Notably, our studies have shown that Syk inhibitors can be used as a potential agent to reduce Gem-induced immunosuppression in the PDAC TME. It has been reported before that multiple doses of clinical Gem treatment regimen can induce an immunosuppressive TME and hampers CD8+ T cell activity in PDAC tumors (46). This study has shown that treatment of KPC GEMM mice with 100 mg/kg dose of Gem for two weeks, lead to an increase in PDL1 expression and an increase in the expression of IL1, CCL2 and TGF β (46). Similarly, Wu et al have shown that multiple doses of clinical Gem treatment regimen induce immunosuppressive TME, although the tumor growth was delayed in the E0771-tumor bearing mice (47). In our studies, we used a low dose of Gem as reported before (10) and found that Gem reduced tumor growth but induced immunosuppressive transcriptional programming in macrophages leading to diminished cytotoxic T cell activity in PDAC tumors. These observations are similar to previous studies demonstrating that PI3Kγ and BTK inhibitors suppress macrophage polarization and improve responses to gemcitabine in PDAC (10,11).

Interestingly, we also observed that Gem treatment reduced the infiltration and activation of CD8+ T cells. Though the effect of Gem on T cells has not been widely explored (48), one study has shown that Gem treatment reduced CD4+, CD8+T cells in a non-small lung cancer mouse model (49) and another study has shown that CD3+ T cells and memory T cells decrease in gem-treated PDAC patients after second and third infusions (50). Our studies on orthotopic mouse models showed that R788 reinvigorates cytotoxic T cells by reducing macrophage-mediated immunosuppression, and combining R788 with Gem eliminated the inhibitory effects of Gem in T cell-dependent manner. Surprisingly, we also observed increased CD8+ T cells in R788-treated slices *ex vivo*. Similar to our observations in *in vivo* models, R788 might have increased the proliferation and reactivation of endogenous tumor reactive CD8+ T cells.

Taken together these studies establish a paradigm that Syk has a crucial role in regulating macrophage- mediated immunosuppression in PDAC tumors and concomitantly in calibrating the effective anti-tumor immune responses in these tumors. Syk inhibitors have long been used in the treatment of B-cell malignancies. However, Syk inhibitors including FDA approved drug fostamatinib (R788) have never been tested in patients with PDAC. The data presented in this manuscript prompt the hypothesis that fostamatinib in combination with gemcitabine may be an effective therapeutic strategy for PDAC that could be rapidly tested in clinical trials.

Acknowledgements: We would like to acknowledge UCSD histology core and UCSD microscopy core. This work was supported by NIH grants K22 CA229594, R01NS122835 to Shweta Joshi and Pediatric Padres Pedal award to Shweta Joshi as well as The Fund to Cure Pancreatic Cancer and Ride the Point to Andrew M. Lowy. This work was also supported by NIH grants: R01CA154480, R01CA121941, R01CA247551, U01CA176058, R01DE026870, U24CA220341, U24CA248457, R01CA226803, U01CA217885 and R01CA109467, a State of California Initiative to Advance Precision Medicine award (OPR18112) to Pablo Tamayo, and the GCBSR shared resources at the UCSD Moores Cancer center P30CA023100.

Author's Contributions: D. Rohila: Conceptualization, data curation, formal analysis, investigation, visualization, methodology, writing-original draft, writing–review and editing. **In Hwan Park:** Conceptualization, data curation, formal analysis, visualization, methodology, writing-original draft, writing–review and editing. **Tim**

Pham: Data curation, formal analysis, visualization, methodology, software, writing-original draft, writing–review and editing. **J. Weitz:** Conceptualization, investigation, methodology, writing-original draft, writing–review and editing. **T. Mendoza:** Data curation, formal analysis, methodology, writing–review and editing. **S. Madheswaran:** Data curation, formal analysis, methodology, writing–review and editing. **M. Ishfaq**: Data curation, formal analysis, methodology, writing–review and editing. **C. Beaman:** Data curation, formal analysis, methodology, writing–review and editing. **E. Tapia:** Data curation, formal analysis, methodology, writing–review and editing. **S. Sun:** Data curation, formal analysis, methodology, writing–review and editing. **J. Patel:** Data curation, formal analysis, methodology, writing–review and editing. **P. Tamayo**: Conceptualization, resources, supervision, funding acquisition, validation, investigation, writing-original draft, writing–review and editing. **A. Lowy:** Conceptualization, resources, funding acquisition, supervision, validation, investigation, writing-original draft, writing–review and editing. **S. Joshi:** Conceptualization, resources, methodology, data curation, software, formal analysis, investigation, visualization, supervision, funding acquisition, project administration, writing-original draft, writing–review and editing.

References:

1. Rawla P, Sunkara T, Gaduputi V. Epidemiology of Pancreatic Cancer: Global Trends, Etiology and Risk Factors. World J Oncol **2019**;10:10-27
2. McGuigan A, Kelly P, Turkington RC, Jones C, Coleman HG, McCain RS. Pancreatic cancer: A review of clinical diagnosis, epidemiology, treatment and outcomes. World J Gastroenterol **2018**;24:4846-61
3. Siegel RL, Miller KD, Fuchs HE, Jemal A. Cancer statistics, 2022. CA Cancer J Clin **2022**;72:7-33
4. Conroy T, Desseigne F, Ychou M, Bouche O, Guimbaud R, Becouarn Y*, et al.* FOLFIRINOX versus gemcitabine for metastatic pancreatic cancer. N Engl J Med **2011**;364:1817-25
5. Daniel D Von Hoff 1 RKR, Mitesh J Borad, Daniel A Laheru, Lon S Smith, Tina E Wood, Ronald L Korn, Neil Desai, Vuong Trieu, Jose L Iglesias, Hui Zhang, Patrick Soon-Shiong, Tao Shi, N V Rajeshkumar, Anirban Maitra, Manuel Hidalgo. Gemcitabine plus nab-paclitaxel is an active regimen in patients with advanced pancreatic cancer: a phase I/II trial. Volume 29(34):2011.
6. Watt J, Kocher HM. The desmoplastic stroma of pancreatic cancer is a barrier to immune cell infiltration. Oncoimmunology **2013**;2:e26788
7. Schober M, Jesenofsky R, Faissner R, Weidenauer C, Hagmann W, Michl P*, et al.* Desmoplasia and chemoresistance in pancreatic cancer. Cancers (Basel) **2014**;6:2137-54
8. Zhu Y, Knolhoff BL, Meyer MA, Nywening TM, West BL, Luo J*, et al.* CSF1/CSF1R blockade reprograms tumor-infiltrating macrophages and improves response to T-cell checkpoint immunotherapy in pancreatic cancer models. Cancer Res **2014**;74:5057-69
9. Stromnes IM, Brockenbrough JS, Izeradjene K, Carlson MA, Cuevas C, Simmons RM*, et al.* Targeted depletion of an MDSC subset unmasks pancreatic ductal adenocarcinoma to adaptive immunity. Gut **2014**;63:1769-81
10. Gunderson AJ, Kaneda MM, Tsujikawa T, Nguyen AV, Affara NI, Ruffell B*, et al.* Bruton Tyrosine Kinase-Dependent Immune Cell Cross-talk Drives Pancreas Cancer. Cancer Discov **2016**;6:270-85
11. Kaneda MM, Cappello P, Nguyen AV, Ralainirina N, Hardamon CR, Foubert P*, et al.* Macrophage PI3Kgamma Drives Pancreatic Ductal Adenocarcinoma Progression. Cancer Discov **2016**;6:870-85

12. Yang S, Liu Q, Liao Q. Tumor-Associated Macrophages in Pancreatic Ductal Adenocarcinoma: Origin, Polarization, Function, and Reprogramming. Front Cell Dev Biol **2020**;8:607209
13. Peranzoni E, Lemoine J, Vimeux L, Feuillet V, Barrin S, Kantari-Mimoun C*, et al.* Macrophages impede CD8 T cells from reaching tumor cells and limit the efficacy of anti-PD-1 treatment. Proc Natl Acad Sci U S A **2018**;115:E4041-E50
14. Mantovani A, Marchesi F, Malesci A, Laghi L, Allavena P. Tumour-associated macrophages as treatment targets in oncology. Nat Rev Clin Oncol **2017**;14:399-416
15. Rodriguez PC, Quiceno DG, Zabaleta J, Ortiz B, Zea AH, Piazuelo MB*, et al.* Arginase I production in the tumor microenvironment by mature myeloid cells inhibits T-cell receptor expression and antigen-specific T-cell responses. Cancer Res **2004**;64:5839-49
16. Deshmukh SK, Tyagi N, Khan MA, Srivastava SK, Al-Ghadhban A, Dugger K*, et al.* Gemcitabine treatment promotes immunosuppressive microenvironment in pancreatic tumors by supporting the infiltration, growth, and polarization of macrophages. Sci Rep **2018**;8:12000
17. Bulle A, Dekervel J, Deschuttere L, Nittner D, Libbrecht L, Janky R*, et al.* Gemcitabine Recruits M2-Type Tumor-Associated Macrophages into the Stroma of Pancreatic Cancer. Transl Oncol **2020**;13:100743
18. Lankadasari MB, Mukhopadhyay P, Mohammed S, Harikumar KB. TAMing pancreatic cancer: combat with a double edged sword. Mol Cancer **2019**;18:48
19. Wang W, Marinis JM, Beal AM, Savadkar S, Wu Y, Khan M*, et al.* RIP1 Kinase Drives Macrophage-Mediated Adaptive Immune Tolerance in Pancreatic Cancer. Cancer Cell **2018**;34:757-74 e7
20. Joshi S, Liu KX, Zulcic M, Singh AR, Skola D, Glass CK*, et al.* Macrophage Syk-PI3Kgamma Inhibits Antitumor Immunity: SRX3207, a Novel Dual Syk-PI3K Inhibitory Chemotype Relieves Tumor Immunosuppression. Mol Cancer Ther **2020**;19:755-64
21. Joshi S, Singh AR, Zulcic M, Bao L, Messer K, Ideker T*, et al.* Rac2 controls tumor growth, metastasis and M1-M2 macrophage differentiation in vivo. PLoS One **2014**;9:e95893
22. Newland A, Lee EJ, McDonald V, Bussel JB. Fostamatinib for persistent/chronic adult immune thrombocytopenia. Immunotherapy **2018**;10:9-25
23. Layton T, Stalens C, Gunderson F, Goodison S, Silletti S. Syk tyrosine kinase acts as a pancreatic adenocarcinoma tumor suppressor by regulating cellular growth and invasion. Am J Pathol **2009**;175:2625-36
24. Hingorani SR, Wang L, Multani AS, Combs C, Deramaudt TB, Hruban RH*, et al.* Trp53R172H and KrasG12D cooperate to promote chromosomal instability and widely metastatic pancreatic ductal adenocarcinoma in mice. Cancer Cell **2005**;7:469-83
25. Andrews FH, Singh AR, Joshi S, Smith CA, Morales GA, Garlich JR*, et al.* Dual-activity PI3K-BRD4 inhibitor for the orthogonal inhibition of MYC to block tumor growth and metastasis. Proc Natl Acad Sci U S A **2017**;114:E1072-E80
26. Joshi S, Singh AR, Liu KX, Pham TV, Zulcic M, Skola D*, et al.* SF2523: Dual PI3K/BRD4 Inhibitor Blocks Tumor Immunosuppression and Promotes Adaptive Immune Responses in Cancer. Mol Cancer Ther **2019**;18:1036-44
27. Seo YD, Jiang X, Sullivan KM, Jalikis FG, Smythe KS, Abbasi A*, et al.* Mobilization of CD8(+) T Cells via CXCR4 Blockade Facilitates PD-1 Checkpoint Therapy in Human Pancreatic Cancer. Clin Cancer Res **2019**;25:3934-45
28. Weitz J, Hurtado de Mendoza T, Tiriac H, Lee J, Sun S, Garg B*, et al.* An ex-vivo organotypic culture platform for functional interrogation of human appendiceal cancer reveals a prominent and heterogenous immunological landscape. Clin Cancer Res **2022**
29. Badea L, Herlea V, Dima SO, Dumitrascu T, Popescu I. Combined gene expression analysis of whole-tissue and microdissected pancreatic ductal adenocarcinoma identifies genes specifically overexpressed in tumor epithelia. Hepatogastroenterology **2008**;55:2016-27
30. Dobin A, Davis CA, Schlesinger F, Drenkow J, Zaleski C, Jha S*, et al.* STAR: ultrafast universal RNA-seq aligner. Bioinformatics **2013**;29:15-21
31. Patro R, Duggal G, Love MI, Irizarry RA, Kingsford C. Salmon provides fast and bias-aware quantification of transcript expression. Nat Methods **2017**;14:417-9
32. Love MI, Huber W, Anders S. Moderated estimation of fold change and dispersion for RNA-seq data with DESeq2. Genome Biol **2014**;15:550

33. Anqi Zhu JGI, Michael I Love. Heavy-tailed prior distributions for sequence count data: removing the noise and preserving large differences Bioinformatics **2019**;35
34. Cassetta L, Pollard JW. Targeting macrophages: therapeutic approaches in cancer. Nat Rev Drug Discov **2018**;17:887-904
35. Nielsen SR, Quaranta V, Linford A, Emeagi P, Rainer C, Santos A*, et al.* Macrophage-secreted granulin supports pancreatic cancer metastasis by inducing liver fibrosis. Nat Cell Biol **2016**;18:549-60
36. Mocsai A, Ruland J, Tybulewicz VL. The SYK tyrosine kinase: a crucial player in diverse biological functions. Nat Rev Immunol **2010**;10:387-402
37. Yi YS, Son YJ, Ryou C, Sung GH, Kim JH, Cho JY. Functional roles of Syk in macrophage-mediated inflammatory responses. Mediators Inflamm **2014**;2014:270302
38. Chen SJ, Lian GD, Li JJ, Zhang QB, Zeng LJ, Yang KG*, et al.* Tumor-driven like macrophages induced by conditioned media from pancreatic ductal adenocarcinoma promote tumor metastasis via secreting IL-8. Cancer Med **2018**;7:5679-90
39. Ding M, He SJ, Yang J. MCP-1/CCL2 Mediated by Autocrine Loop of PDGF-BB Promotes Invasion of Lung Cancer Cell by Recruitment of Macrophages Via CCL2-CCR2 Axis. J Interferon Cytokine Res **2019**;39:224-32
40. Pylayeva-Gupta Y, Das S, Handler JS, Hajdu CH, Coffre M, Koralov SB*, et al.* IL35-Producing B Cells Promote the Development of Pancreatic Neoplasia. Cancer Discov **2016**;6:247-55
41. Spear S, Candido JB, McDermott JR, Ghirelli C, Maniati E, Beers SA*, et al.* Discrepancies in the Tumor Microenvironment of Spontaneous and Orthotopic Murine Models of Pancreatic Cancer Uncover a New Immunostimulatory Phenotype for B Cells. Front Immunol **2019**;10:542
42. Das S, Bar-Sagi D. BTK signaling drives CD1d(hi)CD5(+) regulatory B-cell differentiation to promote pancreatic carcinogenesis. Oncogene **2019**;38:3316-24
43. Mace TA, Shakya R, Pitarresi JR, Swanson B, McQuinn CW, Loftus S*, et al.* IL-6 and PD-L1 antibody blockade combination therapy reduces tumour progression in murine models of pancreatic cancer. Gut **2018**;67:320-32
44. Pan Y, Fei Q, Xiong P, Yang J, Zhang Z, Lin X*, et al.* Synergistic inhibition of pancreatic cancer with anti-PD-L1 and c-Myc inhibitor JQ1. Oncoimmunology **2019**;8:e1581529
45. Li E, Huang X, Zhang G, Liang T. Combinational blockade of MET and PD-L1 improves pancreatic cancer immunotherapeutic efficacy. J Exp Clin Cancer Res **2021**;40:279
46. Principe DR, Narbutis M, Kumar S, Park A, Viswakarma N, Dorman MJ*, et al.* Long-Term Gemcitabine Treatment Reshapes the Pancreatic Tumor Microenvironment and Sensitizes Murine Carcinoma to Combination Immunotherapy. Cancer Res **2020**;80:3101-15
47. Wu C, Tan X, Hu X, Zhou M, Yan J, Ding C. Tumor Microenvironment following Gemcitabine Treatment Favors Differentiation of Immunosuppressive Ly6C(high) Myeloid Cells. J Immunol **2020**;204:212-23
48. Mandili G, Curcio C, Bulfamante S, Follia L, Ferrero G, Mazza E*, et al.* In pancreatic cancer, chemotherapy increases antitumor responses to tumor-associated antigens and potentiates DNA vaccination. J Immunother Cancer **2020**;8
49. Nowak AK, Robinson BW, Lake RA. Gemcitabine exerts a selective effect on the humoral immune response: implications for combination chemo-immunotherapy. Cancer Res **2002**;62:2353-8
50. Plate JM, Plate AE, Shott S, Bograd S, Harris JE. Effect of gemcitabine on immune cells in subjects with adenocarcinoma of the pancreas. Cancer Immunol Immunother **2005**;54:915-25

Figure legends:

Fig. 1. Syk positive macrophages accumulate in murine and human PDAC. A-B. Left panel shows IHC or IF staining of human invasive PDAC patient sample and normal pancreas for CD68 (A) and SYK (B) (scale bar = 20 μm). The right panel shows quantification of CD68+ macrophages or SYK+ cells /40X microscopic field in

the tissue sections (n = 3). The tissue sections were stained with DAPI to detect nuclei in Fig. B. Statistical significance was determined by student's t-test, ** $p < 0.01$, **** $p < 0.0001$. **C-D**. Relative SYK mRNA expression in human PDAC as compared to normal pancreas tissue in data set, GSE15471 (C) and single cell RNA-seq data set (CRA001160) (D). Statistical significance was determined by Wilcoxin signed rank test. **E.** Western blot images showing expression of Syk and β actin in cell lines, B cells, T cells, TAMs and BMDMs. **F**. Syk expression in macrophages, B cells and non-immune cells in human PDAC, using single cell RNAseq data set (CRA001160). **G**. Figure shows IF staining of Syk (red) and CD68 (aqua) in a tissue section from human invasive PDAC. The dual positive cells are indicated by arrows; scale bar = 10μm. **H**. FACS quantification of $pSyk^{348+}$ $CD11b^{+}F4/80^{+}$ cells in normal pancreas and KPC1245 PDAC (n = 3). **I**. Immunoblot showing $pSyk^{348}$ activation in Panc02 PDAC TAMs stimulated with Fc gamma ligation, 1 μg/ml LPS or adhered to H296 (ligand for $\alpha_4\beta_1$).

Fig. 2. Macrophage Syk regulates immunosuppression, PDAC growth and metastasis: A. Panc02 and KPC1245 tumors were orthotopically implanted into $Syk^{MC\text{-}WT}$ and $Syk^{MC\text{-}KO}$ mice according to the depicted schema. **B-C.** Left panel shows weights of pancreata containing Panc02 (B) or KPC1245 (C) tumors from $Syk^{MC\text{-}WT}$ and $Syk^{MC\text{-}KO}$ mice. Figs. in the right panel of B and C shows quantification of metastatic nodules in colonic lymph nodes and liver**.** Significance testing was performed by non-parametric t-tests, * $p < 0.05$, ** $p < 0.01$ *** $p < 0.001$, **** $p < 0.0001$. **D**. Representative images showing Trichrome, αSMA and CD31 staining in KPC1245 PDAC tumors (scale bar = 50μm). Left panel shows CD31 quantification. **E.** FACS quantification of CD3+, CD4+ and CD8+ T cells in Panc02 PDAC tumors. **F**. Left panel shows IHC of KPC1245-PDAC tumors for CD3, CD4+ and CD8 (scale bar = 20 μm). Right panel shows immunodetection of T cells/ microscopic field (n = 3). **G**. Upper panel shows IF staining of CD8 (yellow), DAPI (blue), and Ki67 (red) in KPC1245-PDAC tumors. Lower panel shows quantification data. scale bar = 10μm. **H**. mRNA expression of *Ifng*, *Gzm* and *Prf* in orthotopic $Syk^{MC\text{-}WT}$ and $Syk^{MC\text{-}KO}$ Panc02 tumors. Statistical significance was determined using the student *t* test or one-way ANOVA with Tukey's *post-hoc* multiple pairwise testing when analyzing more than two groups, * $p < 0.05$, ** $p < 0.01$ *** $p < 0.001$, **** $p < 0.0001$.

Fig. 3. Syk promotes immunosuppressive programing of macrophages *in vitro* and *in vivo*. A-B. Left panel shows representative FACS plots, and right panel shows FACS quantification of $MHCII^{+}$ TAMs (A) and

638 CD206^{+} TAMs (B) in representative KPC1245 tumors from Syk$^{MC\text{-}WT}$ and Syk$^{MC\text{-}KO}$ mice (n = 4). Cells were
639 gated on CD11b^{+}F4/80^{+}Gr1^{-} TAMs**. C.** Relative mRNA expression of genes in TAMs isolated from orthotopic
640 Syk$^{MC\text{-}WT}$ and Syk$^{MC\text{-}KO}$ Panc02 tumors. **D**. Relative mRNA expression of genes in N.S and IL4 stimulated
641 Syk$^{MC\text{-}WT}$ and Syk$^{MC\text{-}KO}$ BMDMs as determined by RNA sequencing. **E-F.** Relative mRNA expression of genes in
642 R788 treated macrophages polarized with IL4 *in vitro* (E) or KPC1245-TCM induced TAMs *in vitro* (F), **G**.
643 Weight of R788 treated and control treated orthotopic tumors from Syk$^{MC\text{-}WT}$ and Syk$^{MC\text{-}KO}$ mice (n = 5).

644 **Fig. 4. Syk inhibition reduces tumor growth and sensitizes PDAC tumors to gemcitabine: A.** Schemas
645 for the administration of R788 or anti-PDL1 mAb or Gem in Panc02 or KPC1245 tumors. **B-C**. Weights of
646 pancreata from Panc02 (B) and KPC1245 (C) tumors treated with drugs (n = 5) as depicted in schema in Fig.
647 A. **D.** Metastatic nodules in treated KPC1245 (n = 5) PDAC tumors. Significance testing was performed by one-
648 way Anova with Tukey *post-hoc* multiple pairwise testing, ns- not significant, * $p < 0.05$, *** $p < 0.001$. **E**. Weights
649 of pancreata from KPC1242 tumors treated with drugs (n = 5) as depicted in schema. **F.** Images showing
650 Trichrome staining in PDAC tumors (scale bar = 50 μm).

651 **Fig. 5. R788 overcomes Gem-induced immunosuppression and increases cytotoxic T cells in PDAC:**
652 **A-D.** FACS quantification of intratumoral CD45+ cells (A), CD11b+ cells (B), CD11b+Gr1-F4/80+ TAMs (C),
653 and CD206+ TAMs (D) in end-stage KPC1245 tumors (n = 4) from Fig. 4C. **E.** Relative mRNA expression data
654 of immunosuppressive genes in KPC1245 tumors from Fig. 4C (n=3). **F**. Left panel shows IHC of KPC1245
655 PDAC tumors for CD8 (scale bar = 20 μm) and right panel shows quantification of CD8+ cells/40X (n = 3). **G**.
656 Left panel shows IF staining of CD8 (yellow), and Ki67 (red) in KPC1245-PDAC tumors. Right panel shows
657 quantification data, scale bar = 20μm **H**. FACS plots (right panel) and quantification (left panel) of CD3+, CD4+
658 CD8+ T cells, CD44^{+}CD62L^{-}, CD69+ T cells in KPC1245 PDAC. **I**. Relative mRNA expression of *Ifnγ* and
659 *Gzmb* in KPC1245 tumors (n = 3). **J**. Schema showing administration of different drugs together with anti-CD8
660 depleting antibodies (upper panel). Lower panel shows the weight of pancreata containing KPC1245 tumors.
661 Significance testing was performed by one-way Anova with Tukey *post-hoc* multiple pairwise testing, * $p < 0.05$, ** p
662 < 0.01 *** $p < 0.001$, **** $p < 0.0001$.

663 **Fig. 6: R788 remodels immune microenvironment in KPC GEMM PDAC slice culture: A.** Schematic
664 representation of slice culture technique used for generating human and KPC GEMM PDAC slices**. B-H.**

Relative mRNA expression of immune-response genes in the KPC GEMM PDAC slices treated with either 250 nM Gem or 2.5μM R788 or a combination of both drugs. **I**. Concentration of MCP-1 (CCL2) in Gem or /and R788-treated slices. Significance testing was performed by one-way Anova with Tukey *post-hoc* multiple pairwise testing, ns- not significant * $p < 0.05$, ** $p < 0.01$ *** $p < 0.001$, **** $p < 0.0001$.

Fig. 7. R788 reduces the expression of markers associated with immunosuppressive TAMs and augments immunostimulatory responses in human PDAC slice culture *ex vivo*: A-C. Relative mRNA expression of immunosuppressive genes in the human PDAC slices treated with either 250 nM Gem or/ and 2.5μM R788 from patient 1 (A), patient 2 (B) and patient 3 (C). Significance testing was performed by one-way Anova with Tukey *post-hoc* multiple pairwise testing, ns- not significant * $p < 0.05$, ** $p < 0.01$ *** $p < 0.001$, **** $p < 0.0001$. **D-E**. IHC (D) of human PDAC slices derived from donor 1 for CD206+, CD68+ macrophages and CD8+ T cells (scale bar = 20 μm) and quantification of CD68+, CD206+ and CD8+ cells/40X field (E) **F**. IHC of human PDAC slices derived from patient 4 for CD8+ T cells (scale bar = 20 μm).

Fig. 1

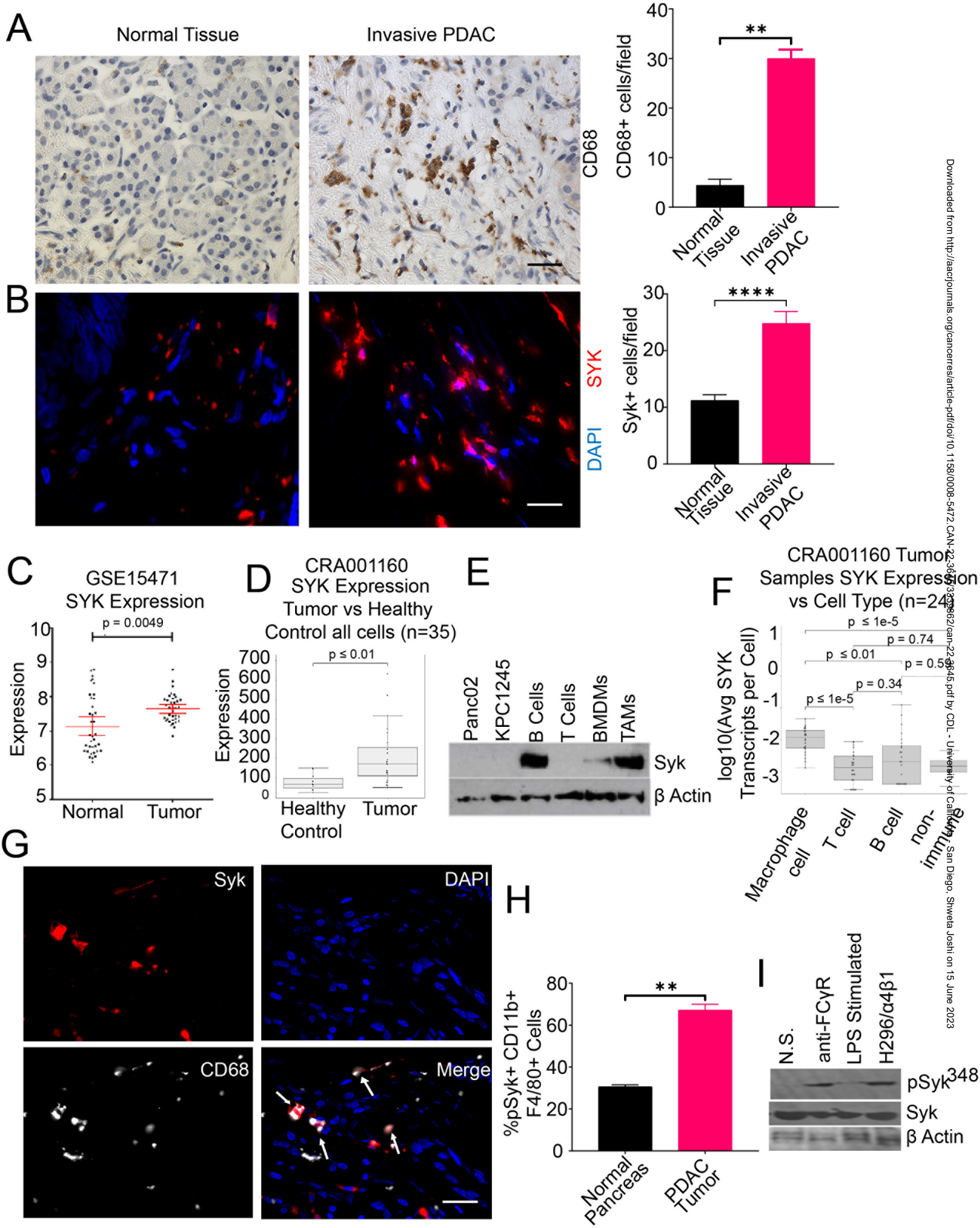

Fig. 2

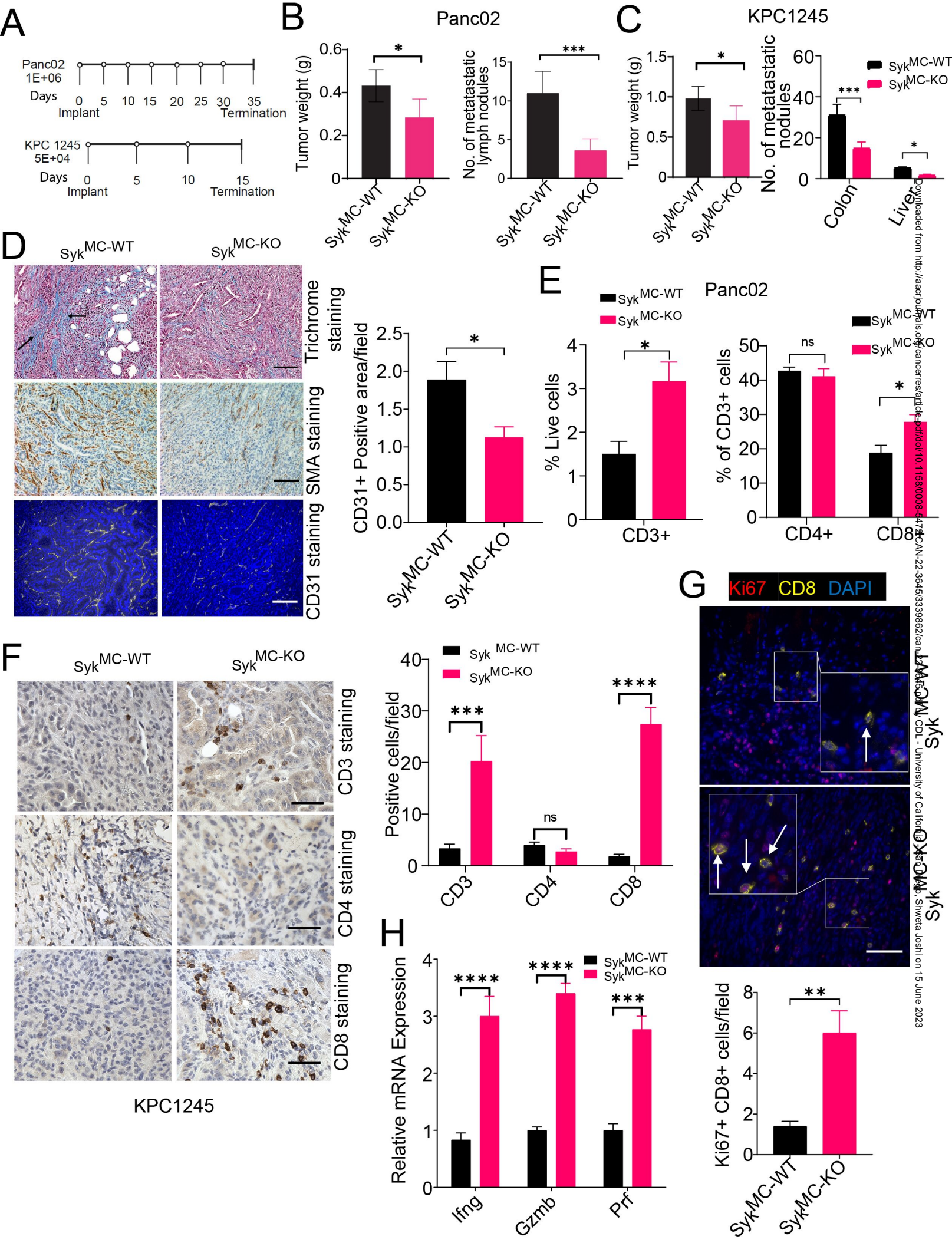

Fig. 3

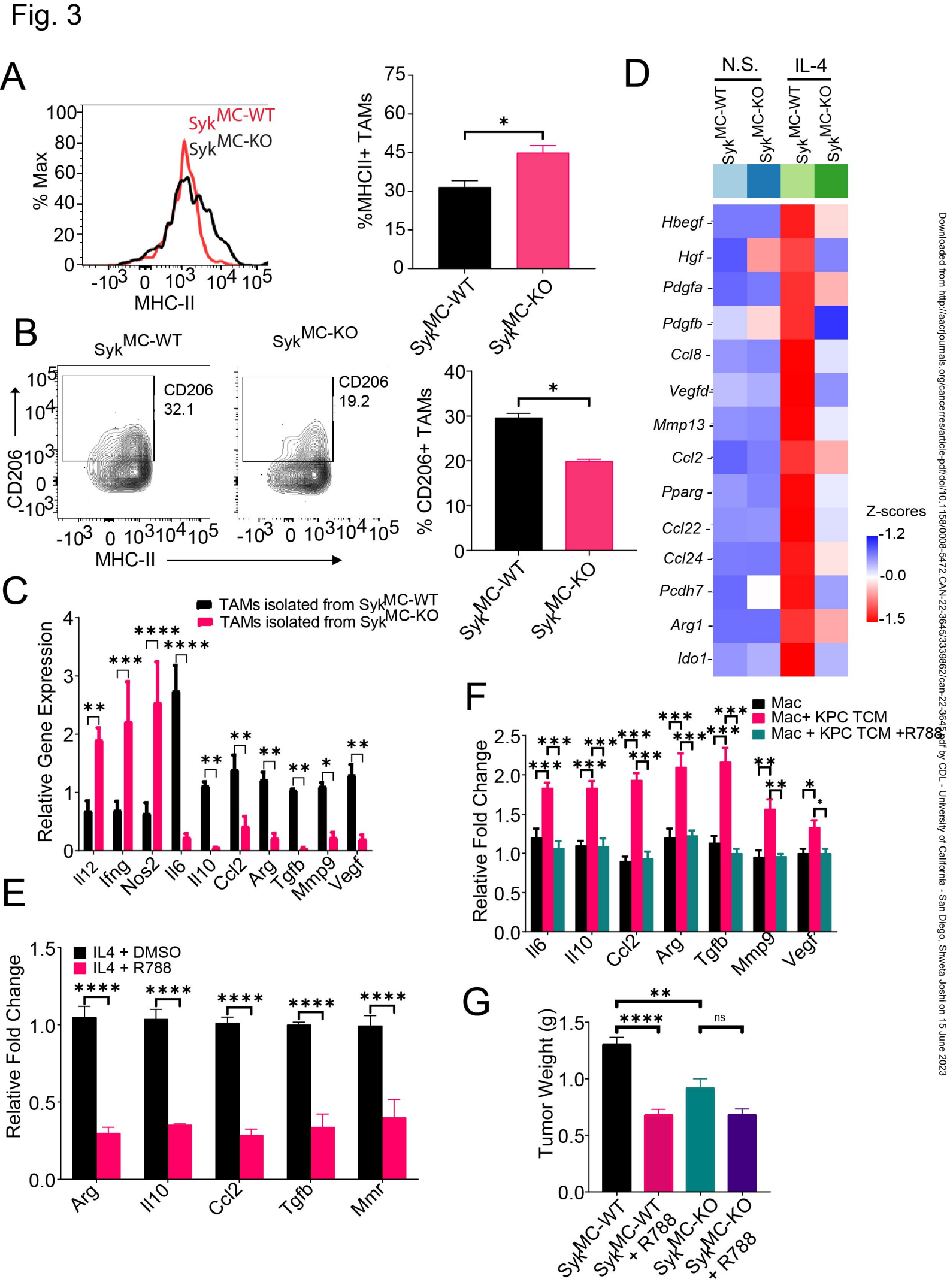

Fig. 4

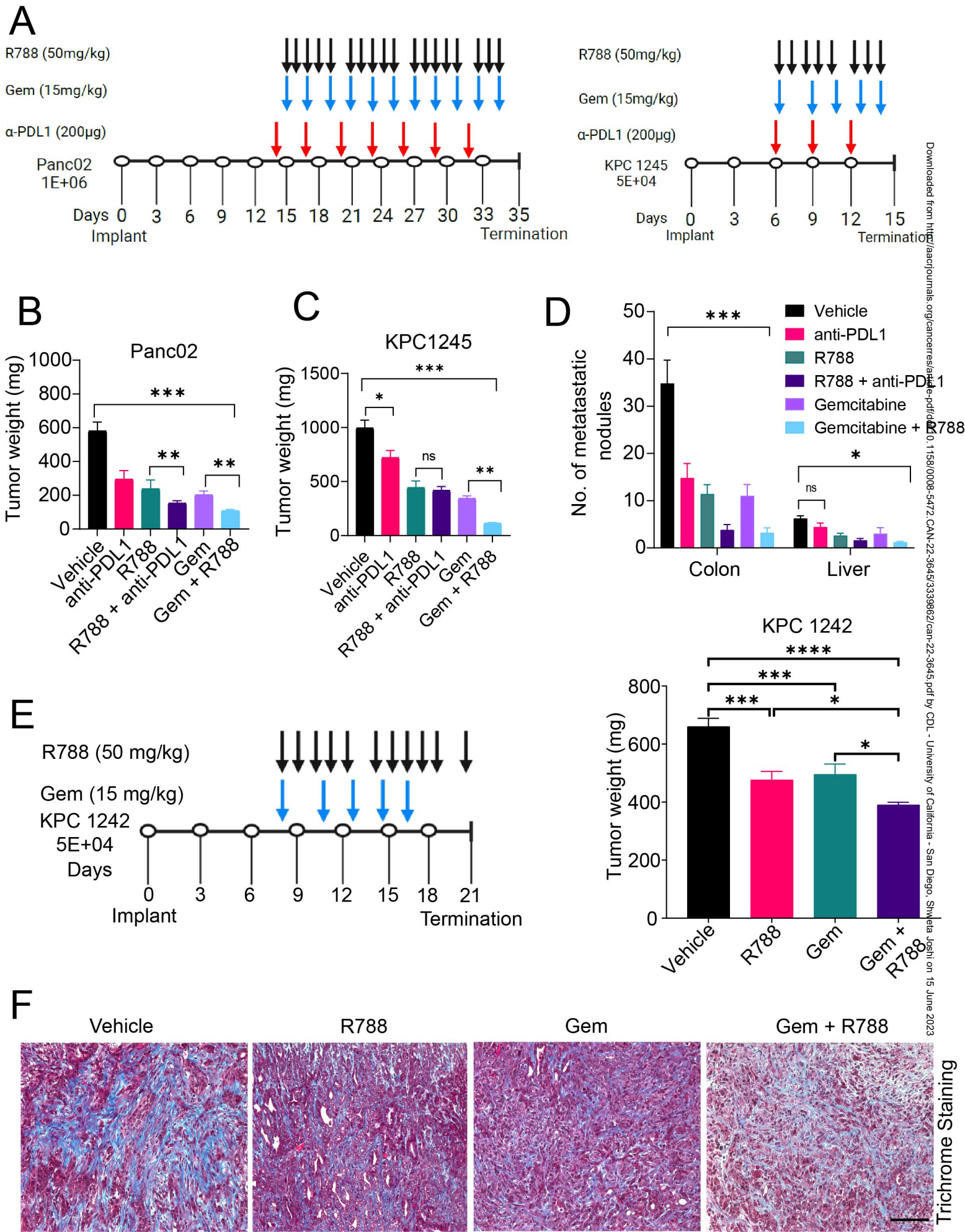

Fig. 5

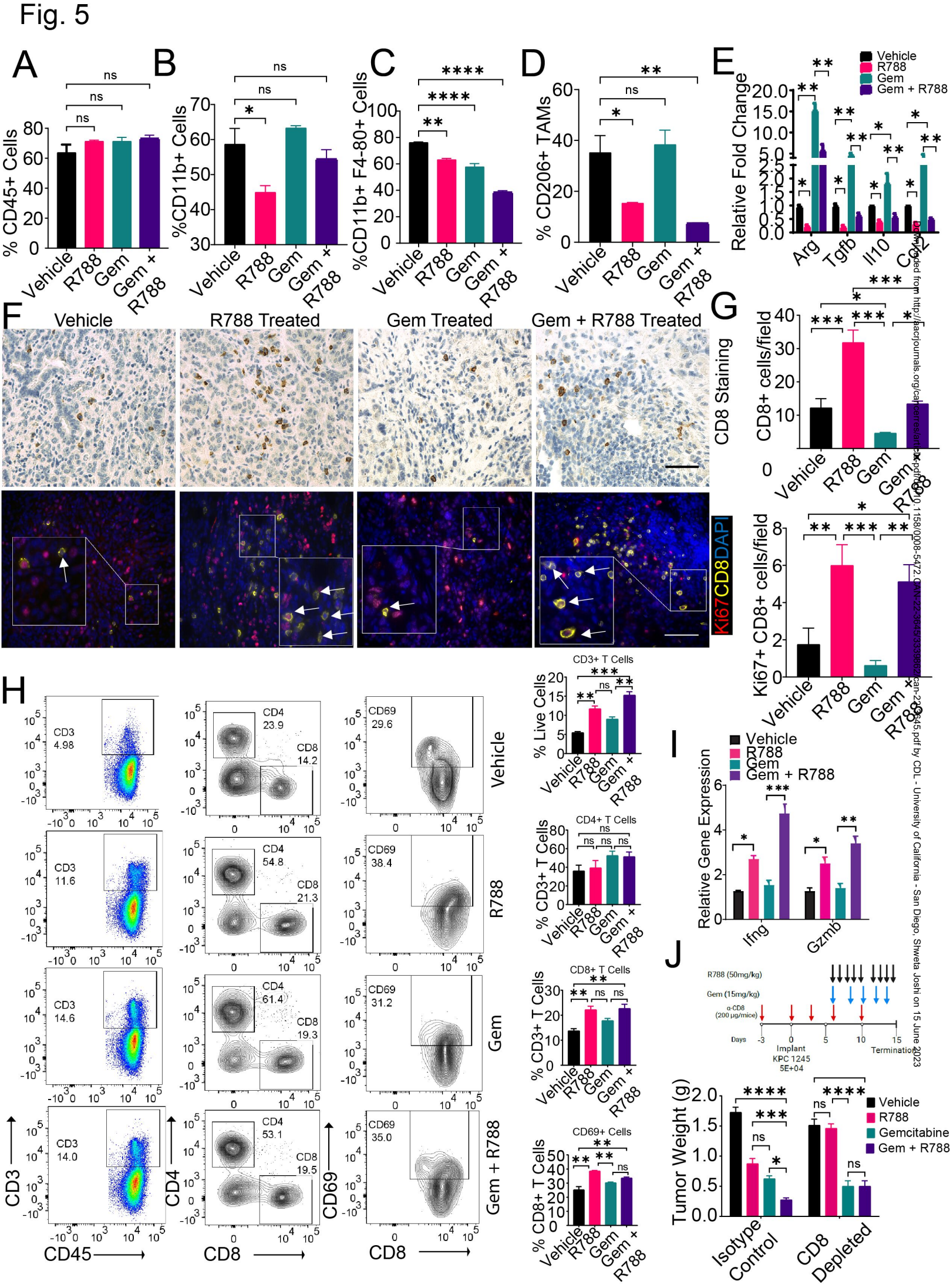

Fig. 6

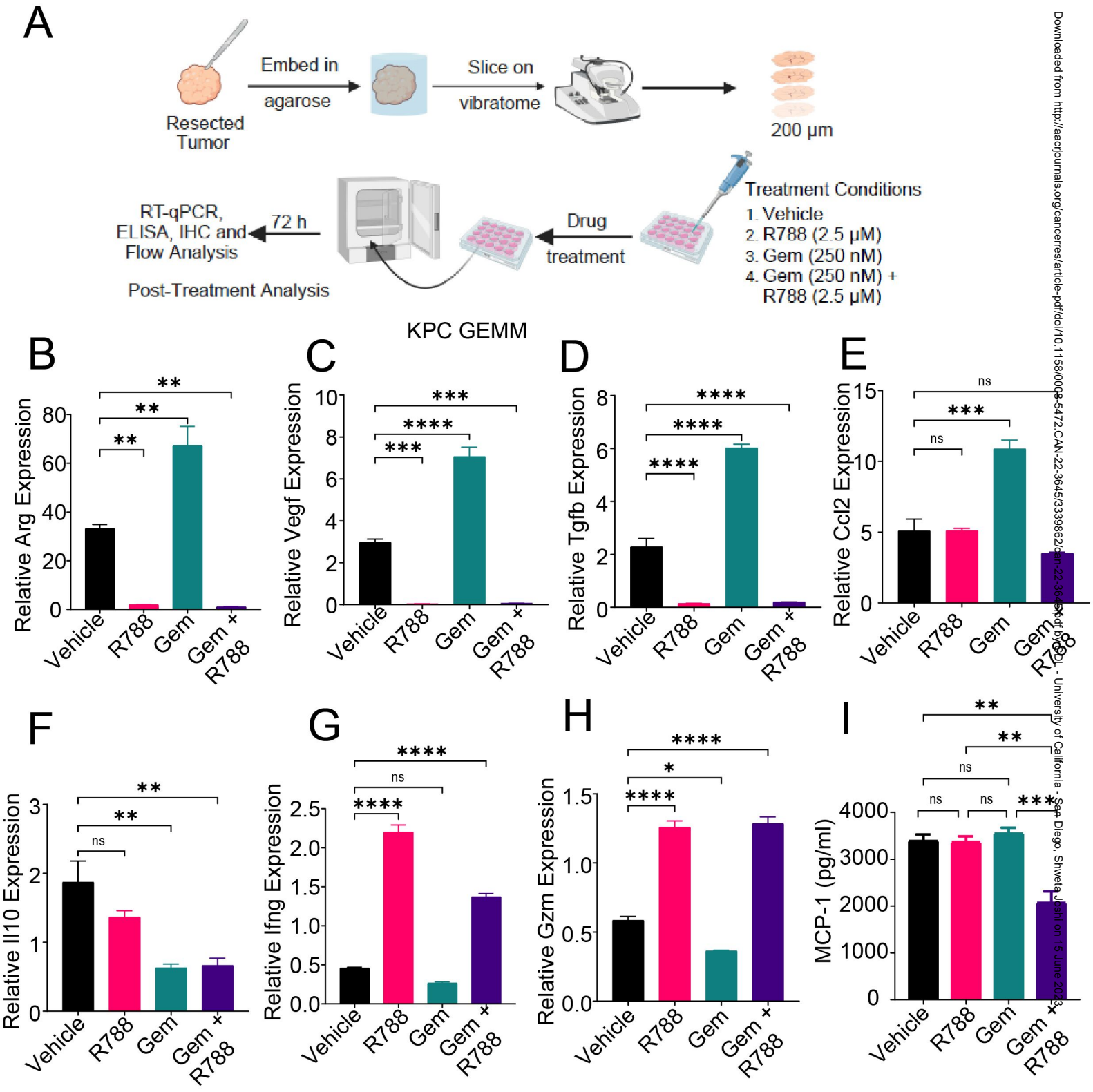
A
Resected Tumor
Embed in agarose
Slice on vibratome
200 µm
Treatment Conditions
1. Vehicle
2. R788 (2.5 µM)
3. Gem (250 nM)
4. Gem (250 nM) + R788 (2.5 µM)
Drug treatment
72 h
RT-qPCR, ELISA, IHC and Flow Analysis
Post-Treatment Analysis
KPC GEMM
B
Relative Arg Expression
C
Relative Vegf Expression
D
Relative Tgfb Expression
E
Relative Ccl2 Expression
F
Relative Il10 Expression
G
Relative Ifng Expression
H
Relative Gzm Expression
I
MCP-1 (pg/ml)
Vehicle
R788
Gem
Gem + R788
ns
Downloaded from http://aacrjournals.org/cancerres/article-pdf/doi/10.1158/0008-5472.CAN-22-3645/3339862/can-22-3645.pdf by UC - University of California - San Diego, Shweta Joshi on 15 June 2023

Fig. 7